Chapter II: Review of Literatures

This chapter discusses the reported literature on structure, magnetic, dielectric and multiferroic properties of $CoCr_2O_4$ spinel as well as transition metal doped $CoCr_2O_4$. Section 2.1.1 discusses the synthesis of $CoCr_2O_4$. Section 2.1.2 summarizes the structure and magnetic properties; section 2.1.3 discusses the dielectric and multiferroic properties of $CoCr_2O_4$. In section 2.2, structure and the properties of transition metals doped $CoCr_2O_4$ are discussed. Section 2.3 presents a vivid view of various magnetic properties, like exchange bias, training effect and memory effect etc. in core-shell nanoparticles.

2.1. Cobalt Chromite Spinel

2.1.1 Synthesis of $CoCr_2O_4$

$CoCr_2O_4$ nanoparticles are synthesized by various techniques like Co-precipitation technique, sol-gel/ citrate gel combustion, hydrothermal processing, low temperature solution combustion and precursor method. Detailed method of synthesis of $CoCr_2O_4$ nanoparticles are reported in this chapter. Some of the popular techniques used for synthesis of $CoCr_2O_4$ are discussed below.

2.1.1.1 Sol-gel auto-combustion method

$CoCr_2O_4$ nanoparticles could be synthesized by sol-gel auto-combustion technique [Hankare et al. (2011)]. The cobalt nitrate, chromium nitrate and citric acid of analytical grade were taken in stoichiometric ratio and were dissolved in deionized water separately. During this process of mixing, the solution was stirred continuously and kept at a temperature of 60 ^oC. Further, ammonia solution was dropped into the mixed solution to adjust the pH value to 7-8. Then the solution was heated slowly to 110 ^oC. Then

change in viscosity is noticed when the sol changes its color into brown puffy dry gel. Then the dried gel was kept under strong combustion process. In order to form the final oxides, these powders were sintered at 800 ^{o}C for 7 h separately in a high temperature furnace.

2.1.1.2 Hydrothermal technique

Hydrothermal method is one of the most useful method which works at high temperature and high pressure. $CoCr_2O_4$ nanoparticles could be synthesized by hydrothermal method [Ptak et al. (2013)]. The precursors of 3.5 mmol of $Co(No_3)_2$. H_2O and 7 mmol of $Cr(No_3)_3.9H_2O$ were taken separately and were dissolved in deionized water separately. These solutions were well mixed together by keeping under continuous stirring. In order to vary the pH of the solution, ammonium hydroxide solution was added drop by drop. The addition of ammonium hydroxide was stopped when pH of the suspension was maintained at 11.7. The obtained suspension was now poured into the teflon reaction vessel. The vessel was kept into a microwave autoclave and heated at 115^{o}C for half an hour. The hydrothermal reaction was subsequently conducted at isothermal condition for five and half hours at 230^{o}C. The autoclave was then cooled to room temperature and the powders were filtered using filter paper. The filtered sample was washed several times with deionized water followed by acetone. Finally, the sample was kept dried in air at 80^{o}C for 20 hours.

2.1.1.3 Sonochemical method

Cobalt chromite can be prepared by sonochemical method [Dimple et al. (2009)]. Rapid reaction rate and controllable reaction conditions are the advantages of this

method. Principle of this technique involves the application of ultrasound energy for the chemical reaction. Cobaltous chloride hexahydrate [$CoCl_2 \cdot 6H_2O$], chromium (III) nitrate nonahydrate [$Cr(NO_3)_3 \cdot 9H_2O$] and ammonia solution of analytical grade were taken separately. An aqueous solution of $CoCl_2 \cdot 6H_2O$ (0.54 g, 2.29 mmol) and $Cr(NO_3)_3 \cdot 9H_2O$ (0.92 g, 2.29 mmol) was taken in 100 ml beaker. Then ammonia (2 ml) was added to the solution drop wise. This system was maintained at room temperature under high intensity ultrasonic (100 W/cm2) radiation for one and half hour with operating frequency of 20 kHz. In order to obtain the required ultrasonic radiation, the titanium horn of 13 nm diameter was immersed to a depth of 6 cm in to the solution. The final temperature reaches to ~60 °C as the reaction cell was not a thermostat. The precipitate was first washed several times with water and then with ethanol after sonication. Then it was kept in centrifuge subsequently. A dark gray powder was obtained which was allowed dried by keeping in a oven. The powders were now heated at 500 °C for 3 hours under nitrogen gas. The black color residue was carefully collected and stored in dry plastic vial.

2.1.2 Structure and magnetic properties

The investigation of classical Heisenberg exchange energy led to the discovery of a new spin state configuration, called ferrimagnetic spiral. This spiral had lowest energy and its configuration was neither Neel type nor Yafet-Kittel type. The ferrimagnetic conical spiral configuration in cubic spinel $CoCr_2O_4$ was first discovered by Menyuk et al. (1964). By considering the ferrimagnetic conical spiral configuration in cubic spinels, Lyons et al. (1962) performed the low temperature neutron diffraction experiment on $CoCr_2O_4$ powders. The results were corroborated with the spiral model of $CoCr_2O_4$

having a normal spinal structure with Curie point T_C ~97 K. They also found the evidence for short- range spiral magnetic order T_S below ~ 86 K, and long-range spiral magnetic order below T_L ~ 31 K. Later, Plumier (1967) reinvestigated the magnetic structure of $CoCr_2O_4$ and found an incommensurate to commensurate transition of the propagation vector. Further, Funahashi et al. (1987) performed the two dimensional neutron diffraction of $CoCr_2O_4$. The results suggested that an incommensurate to commensurate transition occured at about 12.5 K. Kanomata et al. (1988) studied the pressure dependence on the curie temperature of $CoCr_2O_4$ and reported that T_C was shifted from 100.2 K at normal pressure to 103.1 K under 11.5 kbar. Further investigations on magnetic ordering of single crystal $CoCr_2O_4$ was done by Tomiyasu et al. (2004) by neutron scattering experiments. They showed the simultaneous formation of a long-range ferrimagnetic and short-range spiral component in the lowest temperature phase. The long range ferrimagnetic magnetic order was observed below 93 K which caused a spontaneous magnetization of 0.3 μ_B/f.u. They proposed the weak magnetic geometrical frustration. Even if the magnetic ions occupy the A site, then the magnetic geometrical frustration among the B site forms the pyrochlore lattice. This weak geometrical frustration led to the spiral order of short-range and an incommensurate short-range order observed below 50 K which persisted up to 8 K with correlation length, 3.1 nm. Magnetic phase diagram of $CoCr_2O_4$ at low temperature was investigated by Yamasaki et al. (2006). They found that the compound underwent a transition to a conical spin structure with an incommensurate propagation vector at 26 K. Further, in order find out whether the spin-spiral transition, T_S, is long range [Menyuk et al.] or short range [Tomiyasu et al.], Lawes et al. (2006) studied the effect of ferrimagnetic and spin-spiral

transitions on the dielectric constant of polycrystalline $CoCr_2O_4$. A long range ferrimagnetic order have been observed below T_C, 94 K and a sharp phase transition, T_S, 27 K which was ascribed to the onset of long-range spiral order. At 50 K, the development of short-range spiral magnetic order affected the dielectric constant of $CoCr_2O_4$. Li et al. (2006) reported the anomalous magnetic properties in $CoCr_2O_4$ nanocrystals with lattice distortion. The high exchange bias field and large coercivity observed through magnetic measurements were attributed to the lattice distortion and crystal defects along with nanosize effect. Ederer et al. (2007) reinvestigated the theory of ground state spin configuration first presented by Lyons et al. (1962). The significance of AA interactions in AB_2O_4 spinel having magnetic ions on both A and B sites was highlighted in their work. The quantitative prediction of magnetic coupling constants of $CoCr_2O_4$ were obtained using LSDA+U method. They reported that in classical theory of LKDM, the coupling between A-site cations was neglected [Lyons et al. (1962)] which was appreciable in $CoCr_2O_4$. Dutta et al. (2009) studied the magnetic properties of 30-40 nm $CoCr_2O_4$ and reported the long-range ferromagnetic order below 84 K and onset of spiral magnetic order at 25 K which was not sharp. It could be attributed to the finite size scaling effect. The conical spiral order of single crystal $CoCr_2O_4$ was reinvestigated by Chang et al. (2009) and observed a clear long-range ordered incommensurate conical spin state between T_C and T_S. At 26 k, the spin-spiral component with an incommensurate propagation vector was observed. This incommensurate to commensurate conical spin spiral transition was observed at 14.5 K. In incommensurate ordering temperature range, the results were matched with Yamsaki et al. However, the short-range ordering was not observed as claimed by Tomiyasu et al. Rath et al. (2011) reported a superparamagnetic

phase in between para and ferrimagnetic phase in nanoparticles of $CoCr_2O_4$. It was in contrast to paramagnetic to ferrimagnetic phase transition observed in bulk. The high-field magnetic measurements on $CoCr_2O_4$ were studied by Pronin et al. (2012).

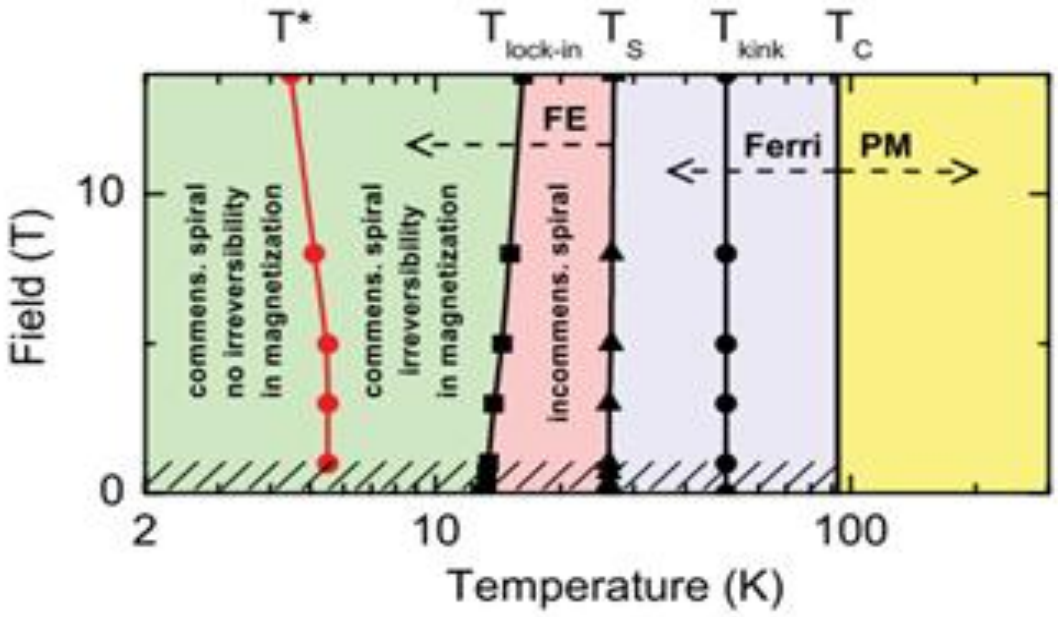

Fig. 2.1.1 The Phase diagram of cobalt chromite based on magnetization, specific heat and literature data. [After Pronin et al. (2012)]

They reported a new phase transition, (T^*) at 5-6 K which was observed below the lock-in transition (T_L) 15-16 K. The phase diagram is shown in Fig. 2.1.1. With decrease in temperature from T_S (26 K), an incommensurate spiral order was observed upto T_L. Further decrease in temperature, below T_L, the sample showed commensurate spiral order with irreversibility in magnetization up to T^*. Below T^*, commensurate spiral configuration showed no irreversibility in magnetization. They also noticed that the applied magnetic field stimulates the irreversibility effect rather than suppresses which could be the reason for appearance of spiral magnetic structure in $CoCr_2O_4$. Later,

Maczka et al. (2013) synthesized 7 nm $CoCr_2O_4$ particles through hydrothermal method and studied the optical and phonon properties in order to investigate the structure and cation distribution of $CoCr_2O_4$. From the diffuse reflectivity study, it was confirmed that cobalt ions appear in octahedral coordination and reported the cation redistribution in $CoCr_2O_4$ with decrease in particle size. In order to study the particle size effects on magnetic properties of $CoCr_2O_4$, Ptak et al. (2013) synthesized nanoparticles of $CoCr_2O_4$ with two different sizes of 23.3 and 4.5 nm. The transition temperature to collinear ferrimagnetic structure occurs at 93-97 K in bulk which was less affected by reducing size to 8 nm. However, by further decreasing the size to 4.5 nm, T_C was decreased to 75 K. They also showed that the incommensurate magnetic structure was developed in particles with mean size of 23.3 nm, below T_S=24 K and which was absent in particles of size 4.5 nm. Further, the magnetic ordering temperatures in polycrystalline $CoCr_2O_4$ were studied by Chen et al. (2013). The magnetization showed irreversibility under thermal cycling, upon cooling the sample from room temperature to 5 K under 100 Oe field and then warming back. The irreversible behavior was not affected by the magnetic field up to 45 kOe which indicated the coexistence of both incommensurate and commensurate spiral orders.

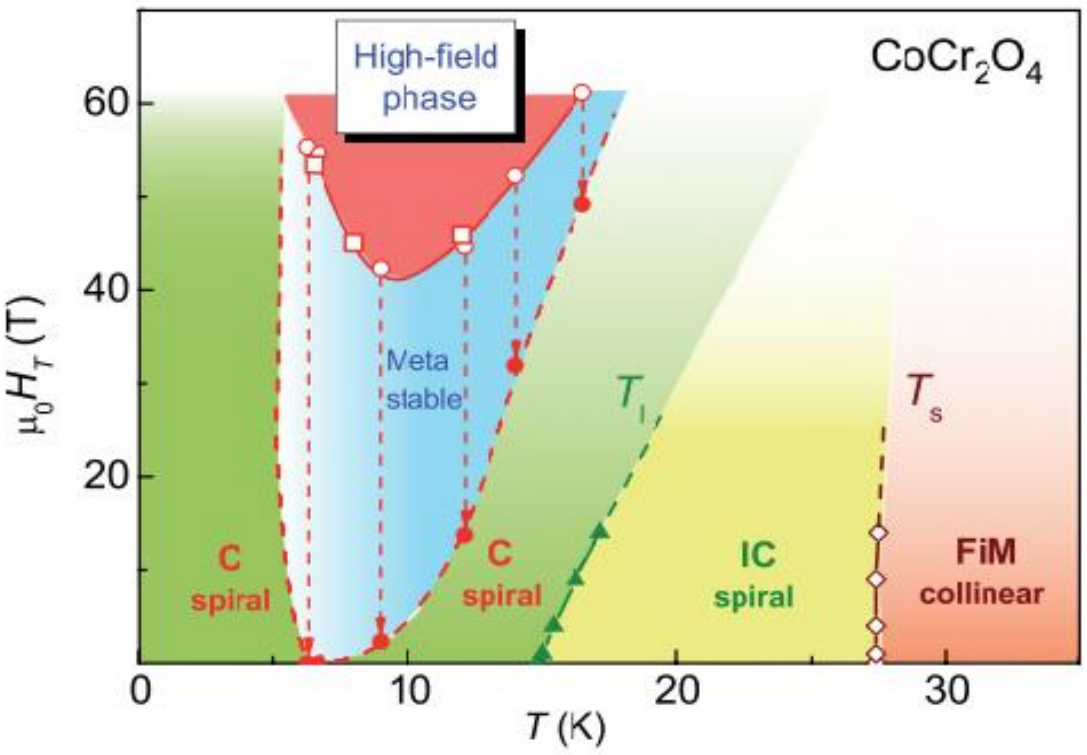

Fig. 2.1.2 Schematic low-temperature phase diagram of $CoCr_2O_4$. [After Tsurkan et al. (2013)]

Tsurkan et al. (2013) studied temperature dependent ultrasound propagation and magnetization of single crystal $CoCr_2O_4$ at high magnetic fields of 62 kOe. They have evidenced different anomalies with clear changes in sound velocity on the commencement of incommensurate-spin-spiral long range order at (T_S) 27 K. The strong spin-lattice coupling in this material was confirmed from the transition from incommensurate to the commensurate state observed at lock-in temperature, T_L, 14 K. They also reported an unconventional magnetostructural state in between 6.2 K to 16.5 K. The state was a high-symmetric and cubic in phase with only the longitudinal component of magnetization being ordered. The long range order of the transverse helical component of magnetization remained disordered. Fig. 2.1.2 show the island of stability of field-induced phase at low temperatures with a minimal critical field of 42 kOe at 9.5 K. Kitani

et al. (2013) reported sharp anomalies at the 13 K which could be due to the strong spin-lattice coupling and was observed in incommensurate phase. Lei et al. (2014) found a simplistic in situ reduction route for the synthesis of polycrystalline nanosheets of $CoCr_2O_4$. The diameters of the nanoparticles were in the range of 20-30 nm. The studies on magnetization showed two low-symmetry ordered states at spiral order transition temperature (T_S) and spin lock-in transition (T_L) along with long-range ferrimagnetic order below the curie temperature (T_C=86 K). However, the specific heat measurements showed no evidence of change in magnetic order from incommensurate to commensurate structure at the lock-in transition, T_L, 13 K. Tian et al. (2015) synthesized 2.8 to 19.7 nm $CoCr_2O_4$ samples using hydrothermal method in order to investigate the size dependent structure and magnetic behavior of $CoCr_2O_4$. Compared to bulk sample, all nanoparticles showed paramagnetic to short-range ferrimagnetic transition with lower T_C at ~ 87 K and there was no magnetic transition was observed around T_S ~ 26 K which revealed the suppression of long-range spiral-spin state. 19.7 nm particles showed enrichment in magnetization when compared with the bulk sample which is unusual. The origin of this enhanced magnetization was explained based on the surface spin structure which strongly affects magnetic behavior in nano particles. The enhanced magnetization was contributed from spontaneous moment of multi-sublattice spin configuration. It was also reported that with reducing particle size, the glass transition temperature (T_g) decreased from 16.3 K for 5.4 nm to 12.8 K for 2.8 nm particles. Karman et al. (2017) synthesized cobalt chromite nanoparticles with average crystallite size of 42 nm by sol-gel method. They observed para to ferrimagnetic transition, T_C at 100 K with conical spiral state at T_S, 27 K and lock-in transition T_L, at 13 K. They reported a negative magnetization of ZFC curve

up to 87 K under 50 Oe field. The negative magnetization was explained by the uncompensated spins at the surface of the nanoparticles which was similar to the reports of Lawes et al. in bulk $CoCr_2O_4$.

2.1.2 Dielectric and multiferroic properties

Yamasaki et al. (2006) observed ferroelectric transition in $CoCr_2O_4$ upon the transition to the conical spin order below 25 K. They demonstrated the multiferroicity in $CoCr_2O_4$ by investigating the presence of ferroelectricity based on the conical spin modulation. The magnetic reversal of ferroelectric polarization confirmed the spontaneous magnetization and multiferroic behavior. In order to validate the multiferrocity in $CoCr_2O_4$, Tomiyasu et al. (2007) carried out the cold neutron scattering experiments on single crystal $CoCr_2O_4$ and studied the size distribution of spiral magnetic clusters by their time scale. The distribution showed the presence of clamping between the ferrimagnetic domains and the ferroelectric clusters. Later, Choi et al. (2009) reported the thermal, magnetic field dependence of the polarization P, magnetization M and spiral wave vector Q in cobalt chromite. This was the first report on the switching behavior of the domains under a varying applied filed and temperature. The switching behavior of a single multiferroic domain was characterized by spiral wave vector Q, in addition to M and P.

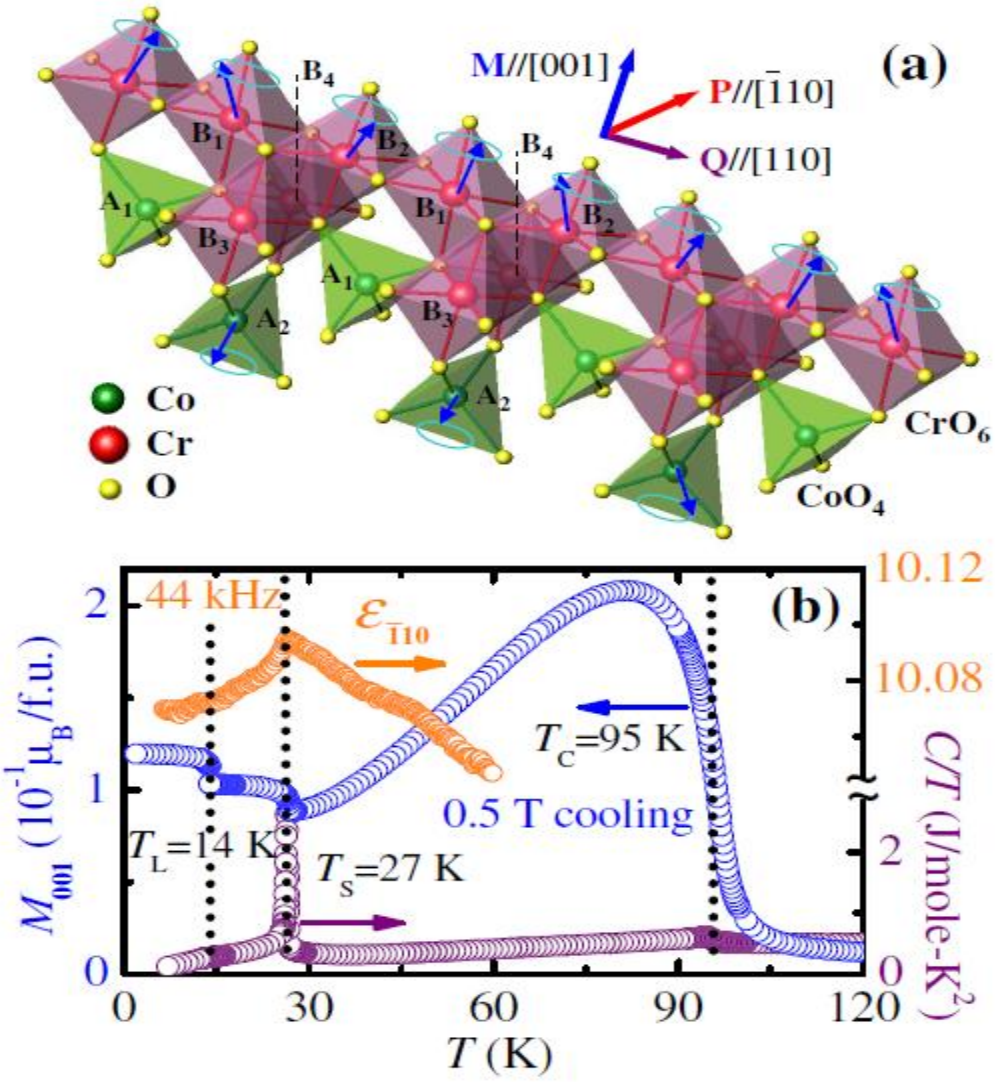

Fig. 2.1.3 (a) Crystallographic and low temperature magnetic structure of $CoCr_2O_4$. (b) Temperature dependence of magnetization, M along [001] direction in 0.5 T filed upon cooling; specific heat divided by temperature under zero field upon cooling and dielectric constant 44 kHz upon warming under zero field. [After Choi et al. (2009)]

The graphical picture of crystallographic and low temperature magnetic spinel structure is shown in Fig. 2.1.3. In contrast to the spiral ordering, where a change in sign of P accompanied a change in sign of Q, P induced by the noncollinear spin order showed a discrete jump with sign change across the lock-in temperature T_L, 14 K without change in Q sign. Further, the strength of the magnetodielectric coupling in polycrystalline

$CoCr_2O_4$ was explained by Mufti et al. (2010) by considering the spin-orbit coupling. The coupling between the magnetic and dielectric properties was observed at the onset of the magnetic spiral structure (T_S) at 27 K and at the lock-in transition (T_L) at 15 K. A small magnetodielectric effect observed in $CoCr_2O_4$ implied that the frustrated materials showed magnetically induced ferroelectricity which do not necessarily show large magnetodielectric properties. Further, in order to find the origin of multiferroicity in $CoCr_2O_4$, Shruti et al. (2010) studied Landau theory for electromagnons. They reported a conical cycloid magnetic phase, below which the ferroelectricity of magnetic origin appears. One of the electromagnon at this phase goes soft and which was responsible for the multiferroicity in $CoCr_2O_4$. Kiran et al. (2011) have studied the multiferroicity in polycrystalline $CoCr_2O_4$ in comparison with $FeCr_2O_4$. They reported that both spinels exhibit polarization in their collinear magnetic state and the structural distortion was due to Jahn-Teller cation (Fe^{2+}) at the A-site which amplifies the polarization of $FeCr_2O_4$ ten times than that of $CoCr_2O_4$. Torgashev et al. (2012) studied the dielectric spectra of $CoCr_2O_4$ in sub-millimeter and infrared (IR) spectral regions in order to unravel the coupling between magnetic and structural properties. They reported the evolution with temperature of exchange optical magnon in the ferrimagnetic (T_C=94 K) and two low-symmetry (T_S≈26K, T_L=14.5 K) phases of $CoCr_2O_4$ down to 5 K in zero magnetic field. It has been shown that the magnon was not a ferrimagnetic in order and originated from spin precession in the cobalt sublattices. The anomalous temperature behavior was observed at the magnetic phase transitions which gave evidence of strong interaction between the magnetic and phonon subsystems. The devices based on materials which show magnetically exchange-coupled were exciting and provide rapid advancing trend

towards device technology. Based on this, Suchomski et al. prepared the highly ordered mesoporous $CoCr_2O_4$ thin films [Suchomski et al. (2011)]. These films have both tunable nanocrystalline domain sizes and uniform 15 nm diameter pores. Magnetization studies on flims with domain size of 10 nm showed both long-range ferrimagnetic order and spiral magnetic order at low temperatures which is in agreement with earlier reports on bulk and polycrystalline samples.

2.2 Transitional Metal Doped Cobalt Chromite

Multiferroic nature was exploited by mixing A and/or B site cations with either magnetic or non-magnetic transition metal ions in various chromites. This section describes the literature review on transition metals doped in A and/or B sites of $CoCr_2O_4$.

2.2.1. Ni doped $CoCr_2O_4$

Polycrystalline $Ni_{1-x}Co_xCr_2O_4$ ($0 \leq x \leq 1$) was synthesized by solid-state reaction. While, $NiCr_2O_4$ show the tetragonal structure with space group, $I4_1/amd$, for $x \geq 0.05$, it showed cubic structure with space group Fd-3m. In the $Ni_{1-x}Co_xCr_2O_4$ compounds, although Co ions mainly occupy the A-site, some of them occupy the B site. The Curie temperatures were noted as 75 K and 90 K for compounds with x=0.2 and 0.8, respectively. Later, the dielectric properties of $Co_{1-x}Ni_xCr_2O_4$ (x=0, 0.2, 0.4, 0.6, 1) solid solution was studied by Bush et al. (2012). They found the evidence of two reversible phase transitions located at 220 K and 245 K for x=0.2. Below 245 K, x=0.2, 0.4 and 0.6 samples manifested pyroelectric properties. For x=0.2, the occurrence of ferrimagnetic transition below 86 K as well as the presence of spontaneous electrical polarization whose direction can be changed by applied field evidenced that the compound posses ferromagnetic in addition

to ferroelectric properties. Hence they became the new members in the family of multiferroics. In order to study the structural properties and strength of spin-phonon coupling in the magnetically ordered phase of $Co_{0.9}Ni_{0.1}Cr_2O_4$ and $CoCr_{2-x}Fe_xO_4$ (x=0.5, 1, 2) polycrystalline powders, temperature dependent magnetic and phonon studies were perfomed by Ptak et al. (2014). They showed that Fe^{3+} doped $CoCr_2O_4$ led to inverted spinel structure which is in contrast with doping of $CoCr_2O_4$ by 10 mol% of Ni^{2+} ions. They reported that doping of 10 mol% of Ni does not have significant change in the magnetic properties. However, the increased Fe^{3+} ion concentration strongly shifted the Curie temperature to 175 K to 340 K and the spin conical phase below T_S was suppressed. Cherepanov et al. (2013) studied the temperature dependent dielectric properties of $Co_{1-x}Ni_xCr_2O_4$:yFe_2O_3 ($0.2\leq x\leq 0.6$) and ($0.01\leq y\leq 0.04$). The spinel structure was cubic at $0\leq x\leq 0.98$ and tetragonal at $0.99\leq x\leq 1$. The compounds with $0.2\leq x\leq 0.6$ exhibited a pyroelectric effect.

2.2.2. Fe doped $CoCr_2O_4$

This section highlights $CoCr_2O_4$ after diluting with Fe ions which has no strong preference either in A or B site of $CoCr_2O_4$. Kumar et al. (2014) observed enhancement of T_C and T_S with increasing Fe concentration at B site of $CoCr_2O_4$. This could be ascribed to the intrinsic change in non-collinear to collinear spin structure. Kochur et al. (2015) have studied cation distribution and valence state of transition metal ions in $Co_{1-x}Fe_xCr_2O_4$ (x=0.1, 0.2, 0.5) using XPS and Mossbauer spectroscopy. Significant Fe^{2+} ions were found in tetrahedral coordination while Fe^{3+} ions were found in both tetrahedral and octahedral sites. They argued that a partly inverse spinel structure in which some of Fe ions substituted Co ions while other Fe ions substituted Cr ions. $CoFe_{0.5}Cr_{1.5}O_4$

nanoparticles studied by Marquez et al. (2012) showed a ferrimagnetic transition at175 K and above this temperature, superparamagnetic nature was suggested. Padam et al. (2013) studied magnetic compensation effect and phase reversal of exchange bias field across compensation temperature in $Co(Cr_{0.95}Fe0.05)_2O_4$. Across the compensation temperature, the sign reversal of exchange bias was reported which was further confirmed from the specific heat measurements. Kumar et al. (2016) reported the size-dependent magnetic orderings in $CoFe_{0.1}Cr_{1.9}O_4$ nanoparticles by magnetic and diffuse neutron scattering using polarized neutrons. With increase in size from 10 to 50 nm, while T_C increased from 110 to 119 K, T_S remained unchanged. In addition to compensation at 34 K, lock-in transition at 10 K was also noticed. In 50 nm particles, a sharp long range ferrimagnetic transition down to 110 K and a short range spiral ordering down to 50 K were observed. While in 10 nm particles, the para to ferrimagnetic transition was found to be continuous, the spiral ordering was diffused in nature. Studies on spin dynamics using different phenomenological models revealed that both particles show spin-glass behavior having higher relaxation time in 10 nm particles than 50 nm. Further, Ram et al. (2016) studied the low temperature neutron diffraction of $Co(Cr_{1-x}Fe_x)_2O_4$ (x=0.05 and 0.075). The ferrimagnetic transition temperature (T_C) was found to increase from 110 K to 118 K with increase in Fe substitution. Neutron diffraction studies revealed that short range magnetic interaction coexist with long range magnetic order below T_C. The short range magnetic order showed unusual non-monotonic temperature dependence. At low temperature, a clear transition into incommensurate spin-spiral phase at T_S was observed when compared to $CoCr_2O_4$. They observed an additional incommensurate modulation in the magnetic structure below T_L, 10 K. Later, Kumar at al. (2017) studied the cation

distribution dependent magnetic properties in $CoCr_{2-x}Fe_xO_4$(x=0.1-0.5) through Extended X-ray Absorption Fine Structure (EXAFS) spectroscopy and Mossbauer measurements. While, the EXAFS spectra showed the preference of Fe ions towards the tetrahedral site at x=0.1, more Fe ions favor towards B site at x=0.5. Further, the quantitative analysis of Mossbauer spectra showed that while 60 % of Fe ions occupy the A side in x=0.1, 40% occupy in x=0.5. But at x=0.3, Fe ions were equally distributed among A and B sites. Magnetic measurements showed while, T_C increased from 102 K to 200 K, T_S increases from 26 K to 40 K with increase in Fe concentration from 0.1 to 0.5.

2.2.3. Zn doped $CoCr_2O_4$

Dwight et al. (1969) showed that five distant-neighbor B-B interactions play crucial role in determining the spin configuration of ground-state of chromite spinels having non-magnetic ions at A.

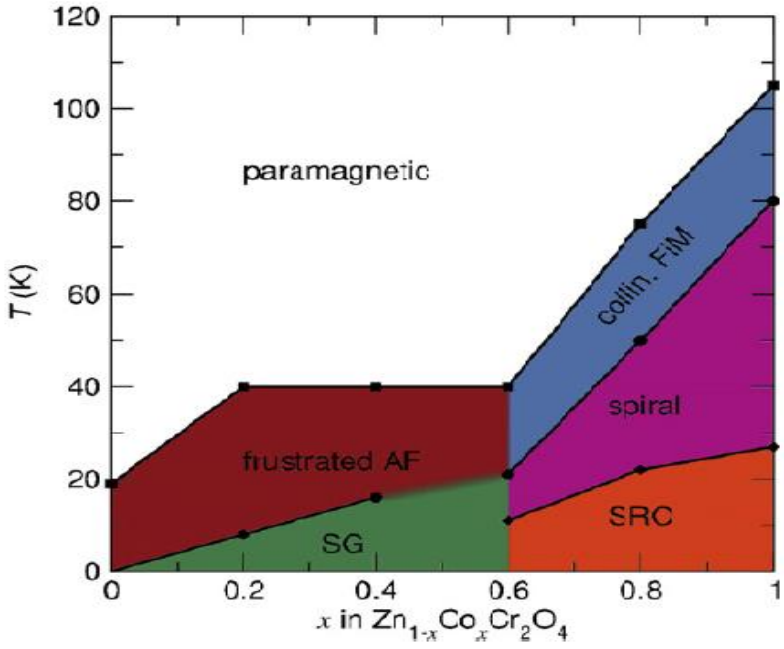

Fig. 2.2.1 Magnetic phase diagram of $ZnCr_2O_4$ as a function of Co content. [After Melot et al. (2009)]

Melot et al. (2009) studied the magnetic properties of complete solid solution of $Zn_{1-x}Co_xCr_2O_4$ (x= 0, 0.2, 0.4, 0.6, 0.8, 1.0). They observed that, introducing a magnetic ion Co, in A site of $ZnCr_2O_4$ resulted in a transition from frustrated antiferromagnetism to glassy magnetism at low concentrations and to ferrimagnetic, conical ground states at higher concentrations. The complete magnetic phase diagram is shown in Fig. 2.2.1. Masrour et al. (2012) obtained the exchange integrals $J_{AA}(x)$ and $J_{AB}(x)$) for $Co_xZn_{1-x}Cr_2O_4$ using theoretical calculations. The high-temperature series expansions combined with pade approximants were used to study the magnetic properties. The obtained absolute values of the exchange interactions $J_{AB}(x)$, $J_{AA'}(x)$ and critical temperatures T_N (x) were shown in Table.2.2.1. It was observed that J_{AB} interaction increased with increase in Co concentration and as a consequence T_N increased.

Table 2.2.1 The absolute values of the exchange interactions and critical temperatures for $Co_xZn_{1-x}Cr_2O_4$. [After Masrour et al. (2012)]

x	$\|J_{AB}\|(x)$	$\|J_{AA}\|(x)$ [19]	$\|J_{AB}\|/\|J_{AA}\|$ (Present work)	$\|J_{AB}\|/\|J_{AA}\|$ (Present work)	T_N	T_N [19]
0.2	31.12	6.72	–	–	11.30	8
0.4	32.27	8.91	3.632	2.583	17.50	15
0.6	33.45	11.67	2.866	0.754	23.60	20
0.8	34.66	15.11	2.293	2.325	60.70	55
1	35.90	19.36	1.818	1.854	82.30	75

Kemei et al. (2014) studied the effect of small amount of magnetic substituents in the tetrahedral sites of the frustrated spinel $ZnCr_2O_4$. The spin-Jahn-Teller distortion observed in $ZnCr_2O_4$ was completely suppressed by the substitution of Co^{2+} ion on the Zn site of $Zn_{1-x}Co_xCr_2O_4$ ($0 \leq x \leq 0.2$). However, the system remained frustrated and magnetic ordering observed at T<20 K.

2.2.4. Other Transition Metal Doped $CoCr_2O_4$

Pankaj et al. (2017) reported the structural, vibrational and dielectric studies of $Co_{1-x}M_xCr_2O_4$ (M=Zn, Mg, Cu and x=0.0, 0.5). They observed that while $CoCr_2O_4$, $Co_{0.5}Mg_{0.5}Cr_2O_4$ and $Co_{0.5}Zn_{0.5}Cr_2O_4$ were found to be cubic, $Co_{0.5}Cu_{0.5}Cr_2O_4$ was found to be in tetragonal structure. Frequency dependent dielectric measurement revealed that dispersion in all chromites could be due to hopping mechanism. The multiferroic, $CoCr_2O_4$ doped by non-JT ion (Zn and Mg) were potential materials for high frequency microelectronics as compared to doped Cu^{2+}, which is a JT active ion. They concluded that doping transitional metal ions in ferrimagnetic spinel chromites does not enhance ferroelectricity. Ram et al. (2018) reported magneto-structural correlation in spinel $Co_{0.8}Cu_{0.2}Cr_2O_4$ using neutron diffraction and magnetic measurements. The Jahn-Teller (JT) active Cu^{2+} ion in the tetrahedral A-site of spinel configuration induced the JT distortion of the crystal structure with a phase co-existence of cubic and orthorhombic at 95 K. They reported that the cubic to orthorhombic distortion completely bypasses the tetragonal one in this compound. Kim et al. (2009) reported that single crystal $CoCr_{2-x}Co_xO_4$ (x=0.0, 0.14, 0.18) display electric polarization reversal behavior below T_S under application of magnetic field. Single crystals of $CoCr_2O_4$ showed enhanced magnetic and ferroelectric properties when Co^{3+} was doped at Cr-site. Both saturation magnetization and electric polarization increased with increase in Co^{3+} concentration from 0.0 to 0.18. Liu et al (2013) prepared $Mn_{1.5-0.5x}Co_{1.5-0.5x}Cr_xO_4$ (0-2) to investigate the cation distribution, thermal expansion at high temperature and electrical properties. With increasing Cr, although the cubic crystal structure was stabilized; the electrical conductivity and coefficient of thermal expansion were decreased. The cation distribution

showed that, while Co had strong preference for the tetrahedral site, Cr and Mn prefer to occupy octahedral sites. Nanocrystalline cobalt doped zinc allu-chromites, $Zn_{1-x}Co_xAlCrO_4$ (x=0.0, 0.25, 0.5, 0.75, 1) were prepared by Hankare et al. (2013) using sol-gel auto-combustion method. The crystallite size and lattice parameters decreased with increase in cobalt content. Two probe resistivity measurements evidenced that the samples were n-type semiconductors. Padam et al. (2014) have studied the exchange bias in non-collinear spin-spiral system $Co(Cr_{1-x}Co_x)_2O_4$ (x=0.0-0.1). The increase in coercivity and noticeable exchange bias was observed only below lock-in-transition T_L. This could be attributed to the presence of commensurate spin-spiral which gets locked to the lattice.

2.3. Magnetic Properties of Core-Shell Nanoparticles

In this section, we have discussed the magnetic properties like exchange bias, training effect, memory effect observed in core-shell magnetic nanoparticles.

Exchange bias was generally expressed as shift in the M-H loop observed when a ferromagnet is in contact with an antiferromagnet. The microscopic origin of exchange bias in core/shell nanoparticles were simulated by Monte Carlo simulations by Oscar Iglesias et al. (2008).

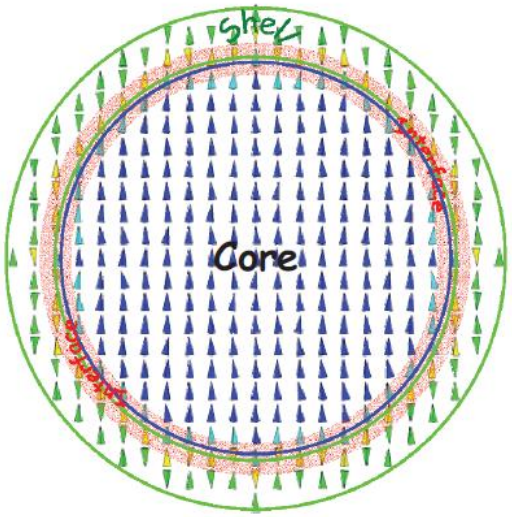

Fig. 2.3.1 Schematic representation of core-shell nanoparticles. The AFM shell showed in green and yellow spins whereas FM core spins are in blue. [After Iglesias et al. (2008)]

The schematic diagram of core-shell structure of nanoparticles and interface interactions are shown in Fig. 2.3.1. The results of the Monte Carlo (MC) simulations were able to account for experimental observations. The obtained field cool (FC) hysteresis loops showed shifts along the field axis which was directly related to the existence of a fraction of uncompensated spins that remain pinned during field cycling at the shell interface. Ali et al. (2007) reported the exchange bias with atypical feature of ferromagnet in contact with a spin glass. A nanogranular system of $CoCr_2O_4$ nanoparticles embedded in Cr_2O_3 matrix has been prepared by Tian et al. (2011) through a high-temperature phase segregation route. Magnetic studies showed a large exchange bias of 1420 Oe and a vertical shift in magnetization of 0.116 emu/g at 10 K. It was observed that the exchange bias decreased with increase in temperature and disappeared at 70 K, while the coercive field initially increased with the temperature upto 40 K and then decreased to zero at 100

K. The exchange bias was explained in terms of exchange coupling between core ferrimagnetic spins and spin glass-like phase at the interfaces. Ali et al. (2007) investigated the exchange bias with strange features of a ferromagnet in contact with a spin glass. They showed that Co/CuMn bilayer system exhibited enhanced coercivity, exchange bias field shifts and training effect associated with a conventional FM/AFM system. The orientation reversal of the bias field just below the blocking temperature, in a small temperature range could be explained using random-field model for long-ranged oscillatory Ruderman-Kittel-Kasuya-Yosida (RKKY) coupled spins. The ferromagnet coupled to a spin glass opens up the door for the study and exploitation of the internal magnetic degrees of freedom like glassy dynamics and ageing phenomena. Vasilakaki et al. (2008) employed the Monte Carlo (MC) simulation method to study the exchange bias effect at an atomic level. In general, the vertical shift and the training effect observed in nanoparticles with a ferromagnetic (FM) core and an antiferromagnetic (AFM) shell. They explained that the interface exchange interaction along with strong interface anisotropy resulted in an exchange bias and coercive field. While the interface of core-shell was responsible for exchange bias, the shell of the nanoparticles contributed to the vertical shift in the magnetization. Evidences of core-shell magnetic behavior was observed by Benitez et al. (2008) in antiferromagnetic Co_3O_4 nanowires. There are mainly two magnetic contributions. One was the regular AFM core which governs the properties of Co_3O_4 nanowires and the other was irreversible magnetization due to the shell of the nanowire. The Monte Carlo simulations performed by Iglesias et al. (2008) revealed the microscopic origin of exchange bias in an individual core-shell nanoparticle. They showed that the increase in exchange coupling across the core-shell interface led to

an increase in exchange bias. The exchange coupling at the interface J_{Int} was independent of its sign and its interface nature. Guo et al. (2009) reported an unconventional exchange bias in $CoCr_2O_4/Cr_2O_3$ nanoparticles. The curie temperature, T_C of $CoCr_2O_4$ was much lower than the Neel temperature of antiferromagnetic Cr_2O_3 and large coercivity was due to fine grains and/or exchange coupling at the interface of antiferromagnetic Cr_2O_3 and ferrimagnetic $CoCr_2O_4$. A negative exchange bias field of 2.5 kOe at 5 K was achieved upon cooling in a field of 30 kOe. The effect of the cooling field on the exchange bias (EB) field and coercivity at 10 K was investigated. The unconventional exchange bias was explained using domain-state model and found that the cooling field play a significant role in the formation of interfacial spin configuration for the unconventional exchange bias. Maaz et al. (2009) studied the magnetic response of 26 nm core-shell cobalt ferrite nanoparticles at low temperature. They reported an increase in exchange bias with decrease in temperature and the strong increase in exchange bias was found below 30 K for ± 20 kOe than ± 90 kOe. The slow increase in exchange bias at high field has been attributed to the high field effect on the surface (shell) spins. At low temperature, the shell spins align along the field direction which weakens the core-shell interactions result to reduction in the exchange bias. Guo et al. (2010) studied the exchange bias and training effect in as-milled Ni/NiO nanocomposites in which a negative EB field of 2.2 kOe at 5 K was observed upon cooling in 10 kOe field. The coercivity of Ni nanoparticles was significantly enhanced by coupling with NiO. Bisht et al. (2010) studied the memory and aging effects in NiO nanoparticles of average size 5 nm. The spin glass behavior was confirmed from the aging and memory effects in FC and ZFC protocols. They argued that the freezing of spins at the surface of individual

particles lead to the spin glass nature. Godsell et al. (2011) synthesized oleic acid (OA) capped Ni/$Ni(OH)_2$ core-shell nanoassemblies of average particle diameter ~34 nm and ~ 14 nm. Temperature dependent ac susceptibility (χ' and χ'') were measured with varying frequency from 0.1 to 1000 Hz showed two peaks for each of the sample which was attributed to the core-shell structure. While the first peak observed at ~22 K was attributed to the paramagnetic/antiferromagteic phase transition of the $Ni(OH)_2$ shell, the second peak was due to the Superparamagnetic(SPM) blocking of pure Ni present at core of the nanoparticles. Hakim et al. (2011) reported the low temperature spin-glass-like phase in $ZnFe_2O_4$ which was not a canted AFM in nature. The peak shifting observed from frequency dependent ac susceptibility measurement indicated the spin-glass behavior and was confirmed from aging, rejuvenation and memory effects. Chandra et al. (2012) studied the spin dynamics of Fe/γ-Fe_2O_3 core-shell structure nanoparticles of mean size 10 nm and their role in triggering exchange bias phenomena. They demonstrated memory effect in FC and ZFC protocol associated with superspin glass state below glass transition temperature (T_g) 68 K. The freezing temperatures of the core and shell were estimated from the temperature decay of isothermal remanent magnetization as 48 K and 21 K respectively. The onset of exchange bias was at 35 K when the ferromagnetic core was frozen spins in the ferrimagnetic shell begin to be blocked which resulted in enhanced exchanged coupling. Topkaya et al. (2012) observed surface spin disorder and spin-glass-like behavior in manganese-substituted cobalt ferrite nanoparticles coated with triethylene glycol (TREG). The applied field dependence of the blocking temperatures followed Almeida-Thouless (AT) line (de Almeida and Thouless 1978) which confirmed the presence of spin-glass-like layer in $Mn_{0.6}Co_{0.4}Fe_2O_4$

nanoparticles. Khurshid et al. (2012) studied the surface spin disorder and exchange-bias in polycrystalline hollow maghemite nanoparticles with two distinctly different average sizes of 9.2±1.1 nm and 18.7±1.5 nm. While minor loop of hysteresis loop was observed in 9.2 nm particles, the loop shift observed in 18.7 nm particles manifested an intrinsic exchange bias. They reported the significance of inner and outer surface spin disorder which produce surface anisotropy and EB. The EB tuning in hallow magnetic nanoparticles was well discussed. Further, Monte Carlo (MC) simulation were used to explain the ZFC aging effect of ultra-small $CoFe_2O_4$ nanoparticles of mean size ~ 3nm embedded in Si matrix by Trohidou et al. (2012). They considered spherical nanoparticles of ferrimagnetic core and a disordered surface spins. The spins were assumed to interact through nearest neighbor Heisenberg exchange interaction. They reported spin-glass-like disorder at the surface affects the magnetic properties to the extent that they exhibited aging effect which was further affected by random freezing of surface spins. Further, Vasilakaki et al. (2013) also considered the Monte Carlo simulations to study the dynamic magnetic behavior of an assembly of ferromagnetic core/antiferromagnetic shell nanoparticles. They considered Co nanoparticles in Mn matrix. The simulations showed that the memory dip of a finite width was observed at wait temperature which confirms the spin-glass-like behavior. The depth of the memory dip increases with increasing wait time and it became more pronounced with increase in nanoparticles concentration. They also reported that the interface exchange interaction was an additional source for the frustration which leads to an enhanced of memory effect. Biswas et al. (2014) reported an abnormal consequences of magnetic memory effect in Fe/γ-Fe_2O_3 nanostructure, which were prepared using electrochemical route. Signature of memory effect was

observed below T_G in both FC and ZFC protocols while appearance of memory effect ZFC protocol confirmed the spin-glass like state. Although having a large particles distribution, unusually, the memory effect was absent below T_B even in FC protocol. Hence, they argued that the distribution of particles size leading to broad distribution in relaxation time was not sufficient to observe the memory effect in accordance with previous reports. Barman et al. (2015) studied exchange bias and training effect in polycrystalline $NiCr_2O_4$. They considered the anisotropic exchange interaction between the ferrimagnetic and antiferromagnetic components to explain the exchange bias. Later, the exchange bias in spin glass $CoCr_2O_4$ nanoparticles was reported by Zhu et al. (2015). When the particle size was reduce to 5.4 nm, due to increased spin disorder they observed the spin glass behavior. The spin glass phase provided a pinning force from some frozen spins to the rotatable spins provided by the spin glass phase explained the origin of exchange bias in this system. Kurshid et al. (2015) prepared hallow γ-Fe_2O_3 nanoparticles of outer diameter 14.8±0.5 nm. These nanoparticles showed spin-glass like freezing of both inner and outer surface layers and increased surface-to-volume ratio. A high exchange bias and its training behavior suggested highly frustrated spins at the surface that rearranged much slowly than interior spins. The obtained hysteresis loops revealed that the magnetic behavior was not identical at the inner and outer surfaces. In 15 nm hollow particles, the outer surface spins exhibited higher degree of frustration. In case of hallow magnetic nanoparticles, the inner and outer surface spins played an important role in determining the magnetic behavior and exchange bias. Wang et al. (2015) observed a large exchange bias and training effect in spin-glass-like in $NiCr_2O_4$/NiO. The cycle dependence of large EB field and vertical shift in magnetization at low temperature could

be due to the pinned spins in spin-glass-like phase at the interface. Nadeem et al. (2015) studied the temperature dependence of exchange bias and memory effects and their interdependences in maghemite (γ-Fe_2O_3) nanoparticles. They argued that the ZFC memory effect observed in the sample could be due to either surface spin-glass arouse due to surface disordered spins and/or super spin-glass arouse due to interacting spins at the core. The exchange bias due to core/shell interface interactions did not enhance the memory effect rather reduced the effect due to spin canting at low temperatures. Zhang et al. (2016) studied the origin producing the training effect by proposing a phenomenological model. The exchange bias combine with training effect could be classified in to two types. One was observed as change in the coercive field at the descending branch and other was at the ascending branch of the hysteresis loop with number of loops (n). It was determined by varying pinning magnetization at the descending/ascending branch during the training process.